Defect and Diffusion Forum
ISSN: 1662-9507, Vol. 434, pp 71-80
doi:10.4028/p-Irzu7d

Submitted: 2023-09-29
Revised: 2024-04-16
Accepted: 2024-04-17
Online: 2024-08-22

Investigating Dislocation Arrays Induced by Seed Scratches during PVT 4H-SiC Crystal Growth Using Synchrotron X-Ray Topography

Qianyu Cheng[1,a*], Yafei Liu[1,b], Zeyu Chen[1,c], Shanshan Hu[1,d], Balaji Raghothamachar[1,e], Michael Dudley[1,f], Vladimir Pushkarev[2,g], Kevin Moeggenborg[2,h], Gil Chung[2,i], Edward Sanchez[2,j], Andrey Soukhojak[2,k]

[1]Department of Materials Science & Chemical Engineering, Stony Brook University, Stony Brook, NY 11794 U.S.A.

[2]SK siltron css, 5300 11 Mile Road, Bay City, MI 48611 U.S.A.

[a]qianyu.cheng@stonybrook.edu, [b]yafei.liu@stonybrook.edu, [c]zeyu.chen@stonybrook.edu, [d]shanshan.hu@stonybrook.edu, [e]balaji.raghothamachar@stonybrook.edu, [f]michael.dudley@stonybrook.edu, [g]vladimir.pushkarev@sksiltron.com, [h]kevin.moeggenborg@sksiltron.com, [i]gil.chung@sksiltron.com, [j]edward.sanchez@sksiltron.com, [k]andrey.soukhojak@sksiltron.com

Keywords: scratch, dislocation array, low angle grain boundary, silicon carbide, crystal growth.

Abstract. The influence of seed preparation on crystal defect generation is studied by investigating the effect of damage from surface scratches not completely removed during polishing on the seed crystal on the nucleation and evolution of dislocation arrays. Synchrotron X-ray topography is conducted on several wafers sliced from a PVT-grown 4H-SiC boule. Topographic results in conjunction with ray tracing simulation reveal the generation of TSD/TMD and TED arrays associated with the scratches in the newly grown wafer adjacent to the seed. Configuration transformation of those arrays is observed as these opposite-signed dislocation pairs composing the arrays were affected by the overgrowth of macro-steps when propagating into the newly grown crystal.

Introduction

Silicon carbide (SiC) is a semiconducting material with a wide bandgap and superior electronic and physical properties including high saturation velocity, high breakdown field, and excellent thermal conductivity [1]. These characteristics make SiC an attractive candidate for utilization in extreme applications, such as high voltage, high power, and high temperature devices. However, various crystallographic defects present in the crystal can hamper the device efficacy, which can considerably reduce the performance of SiC devices [2-6]. Therefore, achieving large scale high-quality SiC single crystal fabrication is of great importance for optimizing SiC device performance and expanding its range of applications.

Among all growth techniques, physical vapor transport (PVT) [7-10] is widely adopted as it enables the production of large-scale SiC substrates with a controlled growth rate. As the seed crystal serves as the foundation for the fully grown crystal boule, obtaining a comprehensive knowledge of the defect generation influenced by seed preparation as well as the defect propagation/conversion mechanism during PVT growth holds critical significance.

In this study, the effect of damage from surface scratches not completely removed during polishing on seed crystal on the nucleation and evolution of dislocation arrays is investigated. Several wafers sliced from a PVT-grown 4H-SiC boule grown from a seed containing traces of surface damage associated with scratches were imaged by synchrotron X-ray topography. Analysis of the topographs reveals the generation of both threading screw/mixed dislocation (TSD/TMD) and threading edge dislocation (TED) arrays associated with the scratches in the newly grown wafer adjacent to the seed. These dislocations are gradually transformed into different configurations further down the boule as growth proceeds.

Experiment

Synchrotron X-ray topography experiments were conducted on three 4° off-axis wafers sliced from the same PVT-grown 4H-SiC boule. For each wafer, topograph in $11\bar{2}0$ reflection was recorded using synchrotron white beam X-ray with transmission geometry, Si-face as the beam exit surface. For grazing-incidence geometry using synchrotron monochromatic beam, $11\bar{2}8$ reflection topographs were recorded from the Si-face of the specimen at an energy of 8.99 keV. X-ray topography images were recorded on Agfa Structurix D3-SC films with approximately 1 μm resolution. The experiments were carried out at Beamline 1-BM of the Advanced Photon Source (APS) in Argonne National Laboratory (ANL).

The dislocation nature of defects observed topographically were confirmed by ray tracing simulations [11]. The principle of ray tracing simulation is based on the orientation contrast mechanism [12], where the direction of local diffracted X-ray beams is calculated through the displacement field associated with the defect. The diffracted X-rays are then projected onto the recording plate. The distortion aroused by the presence of a dislocation within the crystal is revealed as dark or white contrast difference due to the superimposition or separation of diffracted X-rays resulted from the inhomogeneous intensity distributions. This simulation approach has demonstrated its ability to characterize different types of dislocations that appeared in various crystals in previous studies [13-18].

Results and Discussion

As shown in the schematic diagram in Fig. 1, the first wafer was sliced at the seed interface and contains part of the seed crystal. The second wafer is adjacent to the first wafer in the newly grown boule while the third wafer was sliced further down the boule. Synchrotron X-ray topographs reveal the presence of linear defect features located at the same position across all three wafers. Fig. 2 demonstrates an example for this observation. A large number of sharp features with linear contrasts at random orientations are found down the lower edge of the wafer on the $11\bar{2}0$ reflection synchrotron white beam X-ray topograph of the first wafer recorded in transmission geometry (Fig. 2a). These contrasts correspond to damage from surface scratches that was not completely removed during polishing. By comparing the grazing-incidence $11\bar{2}8$ reflection synchrotron monochromatic beam X-ray topographs recorded from the other two wafers (Fig. 2b & 2c), two linear defect features following the same scratch orientations approximately 60° and 120° counterclockwise to $[11\bar{2}0]$ appear at the same location on the later grown wafers as indicated by the blue arrows. Only Scratch 1 and Scratch 2 in Fig. 2a show correlated defect features on Wafer 2 and Wafer 3, whereas other scratch contrasts revealed on Wafer 1 present no significant defect feature on later grown wafers. This indicates linear features that have correlated defects at the same location on the newly grown crystal originated before the growth process, were present on the original seed crystal surface, and are present in the wafer's bulk while Wafer 1 was sliced. The other scratches are formed at random locations and orientations after growth during slicing and polishing of the wafer. Note that the use of transmission geometry to record the $11\bar{2}0$ reflection records defects within the entire volume of the crystal and therefore, both defects present in the as-grown boule and created during wafer slicing are imaged.

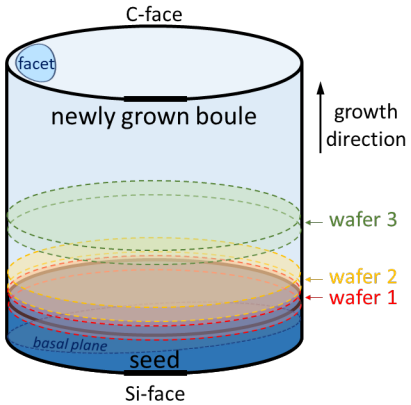

Fig. 1. Schematic diagram of a 4° off-axis 4H-SiC boule showing the slicing position of three wafers being investigated in this study.

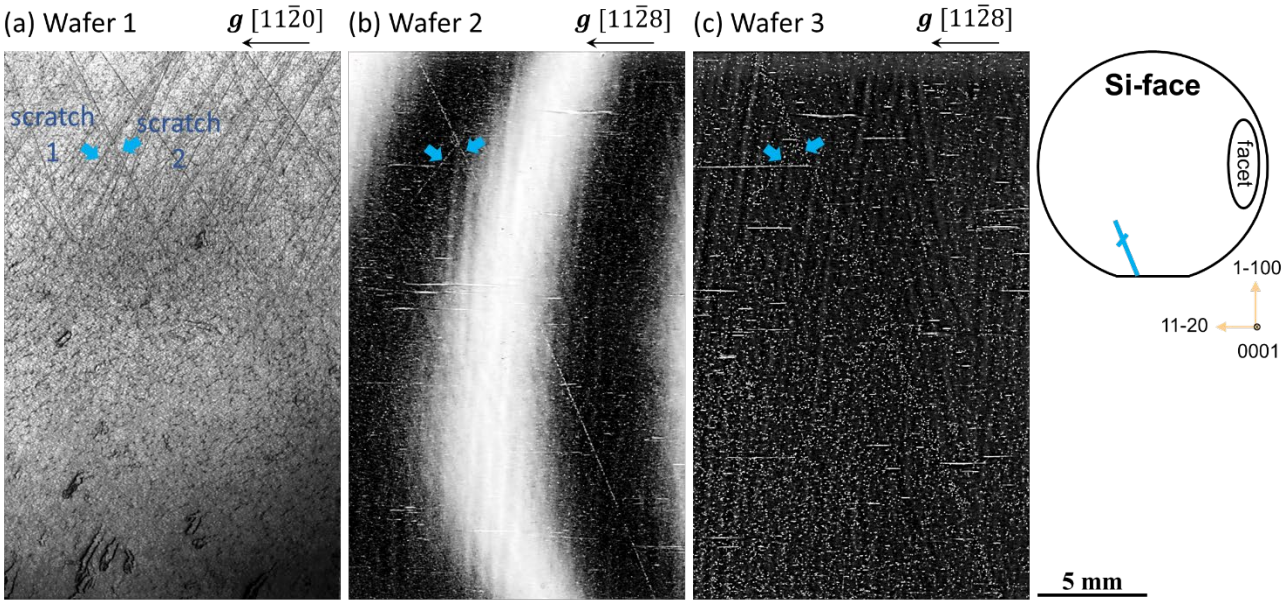

Fig. 2. Synchrotron X-ray topographic observation of scratch related contrast at the same position across (a) Wafer 1; (b) Wafer 2; and (c) Wafer 3 sliced from the same boule. The location of this feature is by the bottom edge of the wafer indicated by the blue line shown on the inset schematic diagram.

Scratch Induced TSD/TMD Arrays. The configuration of scratch induced dislocation is revealed on the enlarged topographs shown in Fig. 3 corresponding to selected regions in Fig. 2b and Fig. 2c. Analysis of the topograph confirmed the generation of dislocation arrays associated with both scratches in the newly grown Wafer 2 adjacent to the seed (Fig. 3a & 3c). However, these dislocation arrays are gradually transformed into different configurations further down the boule as shown in the X-ray topographic images of Wafer 3 (Fig. 3b & 3d). Both dislocation arrays induced by scratches are initially composed of closely spaced TSDs/TMDs as identified by comparing the size and configuration of topographic dislocation contrast with ray tracing simulated results [19]. Those TSD/TMD arrays are observed as distinct narrow linear features positioned at the exact location of the original seed scratch. Further down the boule, those TSD/TMD arrays evolve to spread over a wider area with decreased dislocation density of the array (from 3688 cm^{-2} in Wafer 2 to 3027 cm^{-2} in Wafer 3). Such TSD/TMD array generation due to seed scratch occurs across the whole sample area irrespective of the position or orientation of the scratch as shown in Fig 4 and Fig 5. Fig. 4 shows a scratch induced TSD/TMD array located at the lower right edge of the wafer with inclined linear orientation approximately 15° counterclockwise to [11$\bar{2}$0]. This TSD/TMD array observed the same behavior as the initially closely spaced TSDs/TMDs in the array (Fig. 4b, 4d) in Wafer 2 spreads out in later grown Wafer 3 (Fig. 4c, 4e) with decreased dislocation density. In Fig 5, the enlarged grazing-incidence 11$\bar{2}$8 reflection topographs reveal that dislocations composing TSDs/TMDs arrays are mostly opposite-signed pairs, where the canted white oval TSD/TMD contrast appears in pairs with their white or dark outer arcs facing towards each other. This is confirmed by comparing with ray tracing simulated contrasts of opposite-signed TSD pairs as shown in Fig. 5 inset, where the contrast configuration of paired dislocations in the array (marked by blue circles) correlates well with the results of ray tracing simulated TSD pairs with Burgers vector of opposite-signed and different magnitude combinations.

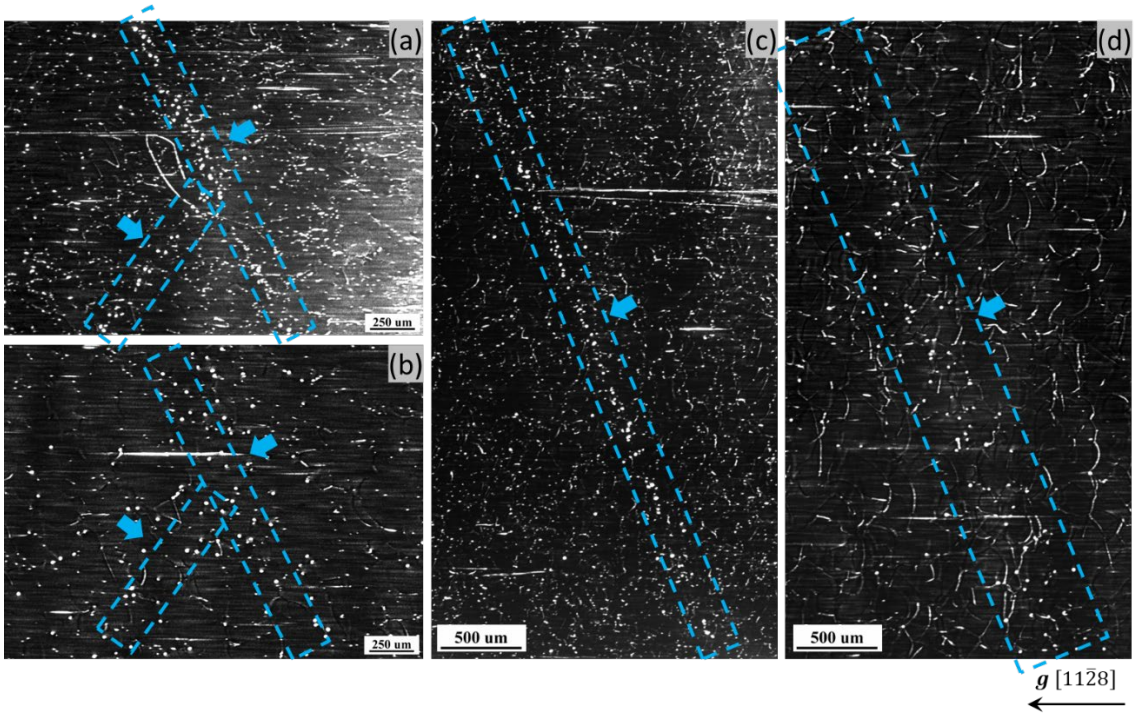

Fig. 3. Enlarged images of 11$\bar{2}$8 reflection synchrotron monochromatic X-ray topographs showing: (a) the intersection of two TSD/TMD dislocation arrays (marked by dashed outline) on Wafer 2 induced by Scratch 1 and Scratch 2 on Wafer 1 in Fig. 2a; (b) the intersection of two TSD/TMD dislocation arrays (marked by dashed outline) on Wafer 3 induced by Scratch 1 and Scratch 2 on Wafer 1 in Fig. 2a; (c) the TSD/TMD dislocation array on Wafer 2 induced by Scratch 2 on Wafer 1 in Fig. 2a; (d) the TSD/TMD dislocation array on Wafer 3 induced by Scratch 2 on Wafer 1 in Fig. 2a.

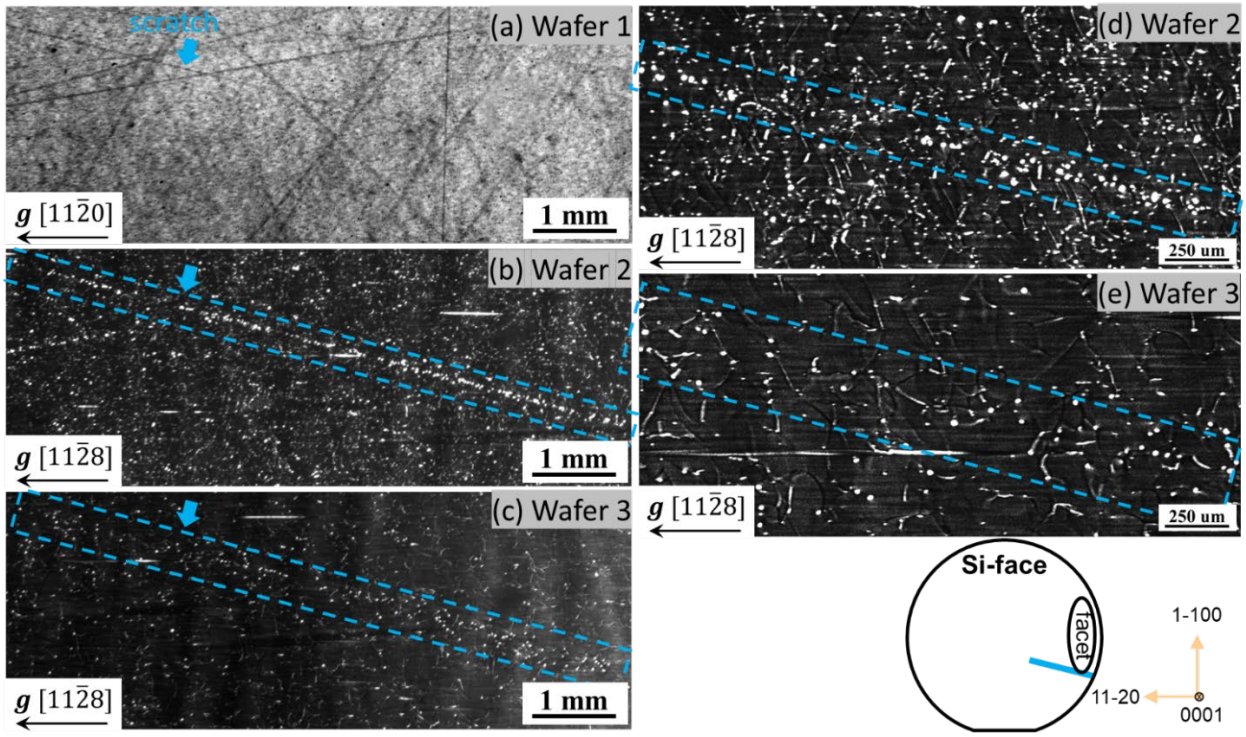

Fig. 4. Synchrotron X-ray topographic observation of scratches on Wafer 1 (a); and correlated TSD/TMD arrays (marked by dashed outline) on Wafer 2 (b, d); and Wafer 3 (c, e). The location of this feature is at the lower right edge of the wafer indicated by the blue line shown on the inset schematic diagram. The dislocation density of this TSD/TMD array decreased from 10579 cm^{-2} in Wafer 2 to 6717 cm^{-2} in Wafer 3.

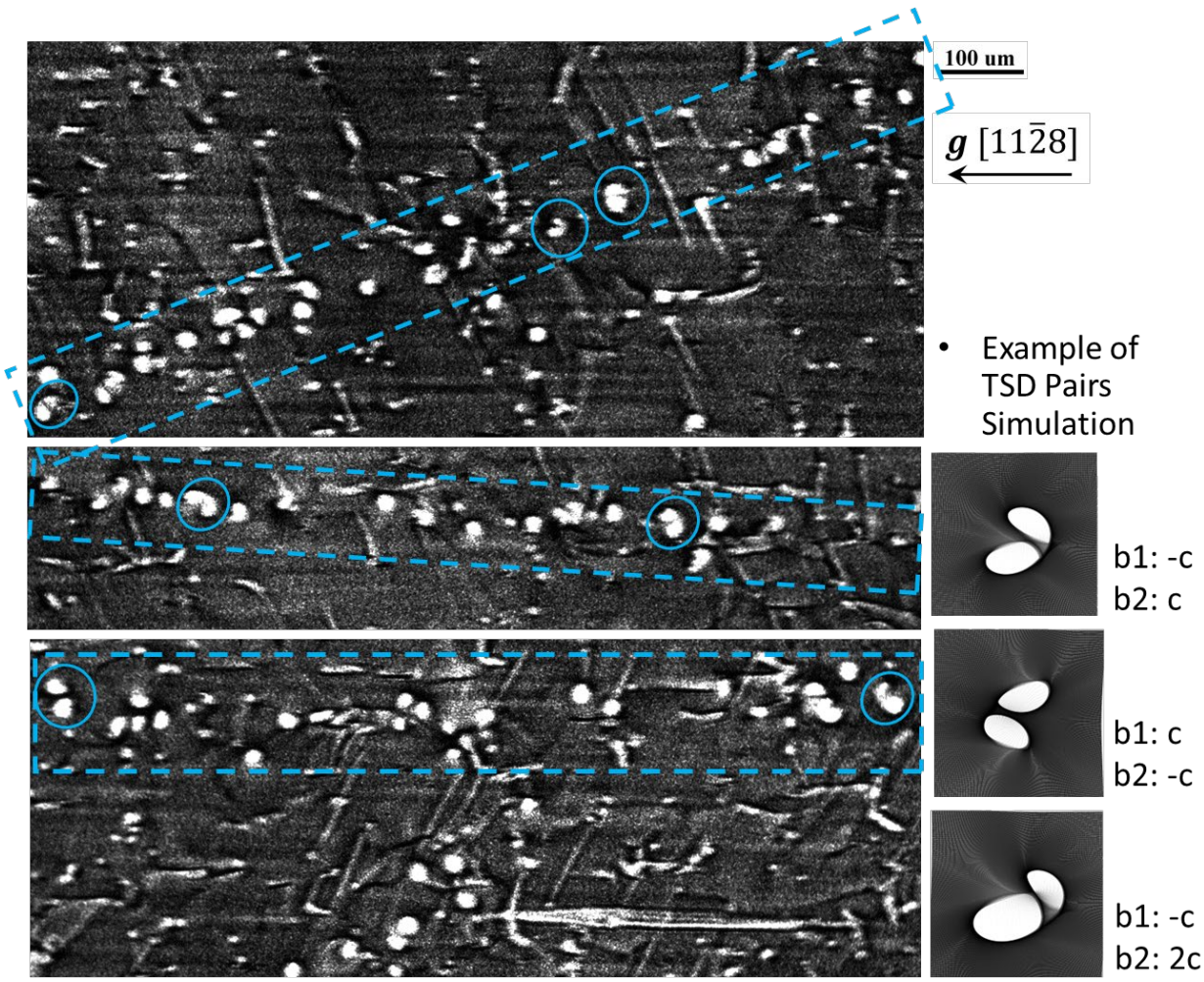

Fig. 5. 11$\bar{2}$8 reflection synchrotron monochromatic beam X-ray topographs of different TSD/TMD arrays showing the appearance of opposite-signed dislocation pairs indicated by blue circles. Some examples of ray tracing simulated TSD opposite-signed pairs are provided inset for configuration comparison.

Scratch Induced TED Arrays. Topographs also revealed the formation of TED arrays associated with scratches in the newly grown crystal with configuration transformation as PVT growth process continues. Fig. 6 shows an example of scratch induced TED array and its evolution during the growth process. This scratch located at the lower inner region of Wafer 1(Fig. 6a) is found to nucleate a TED array (Fig. 6b & 6d) in Wafer 2 at the same location, consisting of closely spaced TEDs along the scratch orientation. Further down the boule in Wafer 3 (Fig. 6c & 6e), the TEDs are observed evolving into a LAGB as TEDs organize along the $< 1\bar{1}00 >$ crystallographic orientations with a zig-zag feature in order to accommodate the initial scratch line direction. Those black and white dot contrasts indicate that TEDs composing the dislocation array/LAGB appear as opposite-signed dislocation pairs. The overall dislocation density of this array/LAGB decreased from 57671 cm^{-2} in Wafer 2 to 39090 cm^{-2} in Wafer 3. This phenomenon is frequently observed across the inner region of the sample. Additional evidence for this observation is provided as shown in Fig. 7, where a scratch located at the upper inner region of Wafer 1 (Fig. 7a) is found inducing dislocation arrays at the same location on the later grown Wafer 2 and Wafer 3 (Fig. 7b, 7c). Enlarged topographs (Fig. 7d, 7e) show those arrays are composed of white and dark contrast opposite-signed TEDs orientated with zig-zag $< 1\bar{1}00 >$ orientations. A reduction in TED density composing the array is found from Wafer 2 in 32223 cm^{-2} to Wafer 3 in 20165 cm^{-2}.

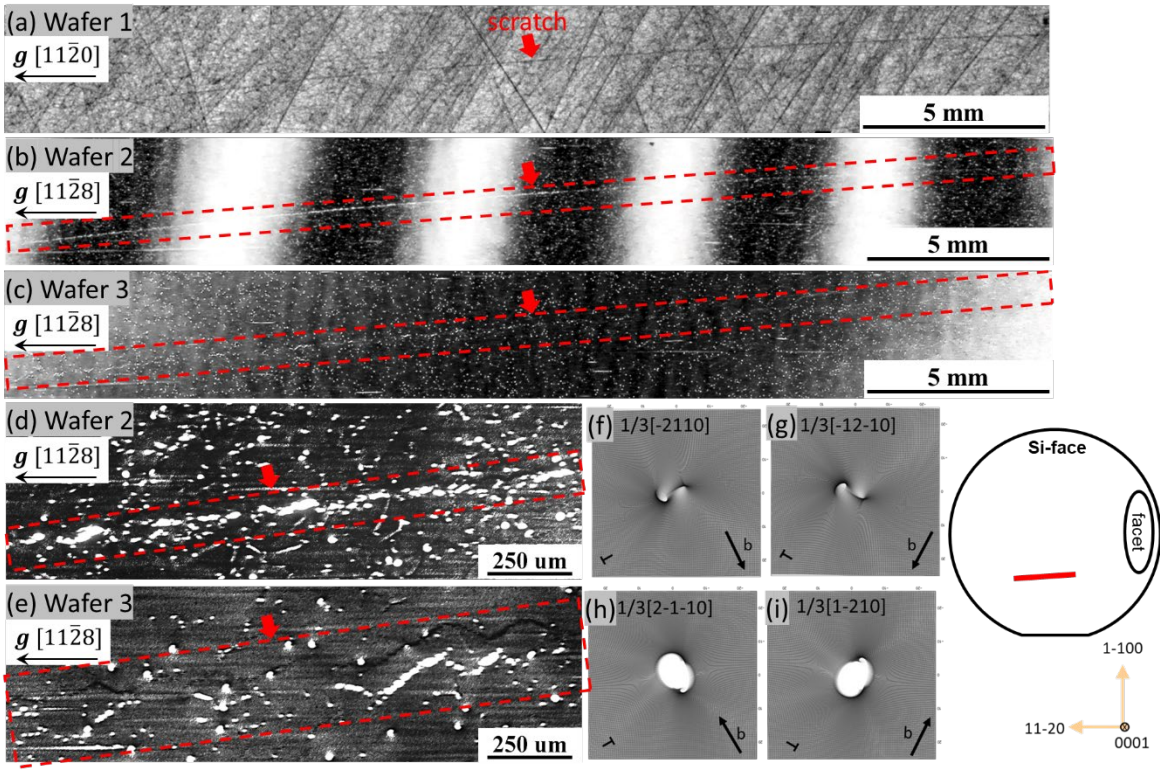

Fig. 6. Synchrotron X-ray topographic observation of a scratch on Wafer 1 (a); and the correlated TED array on Wafer 2 (b, d); and TED LAGB on Wafer 3 (c, e). Ray tracing simulation contrast of TEDs with different Burgers vector indicates the black and white dot contrast are opposite-sign TED pairs (f-i). The location of this feature is at the lower inner region of the wafer indicated by the red line shown on the inset schematic diagram.

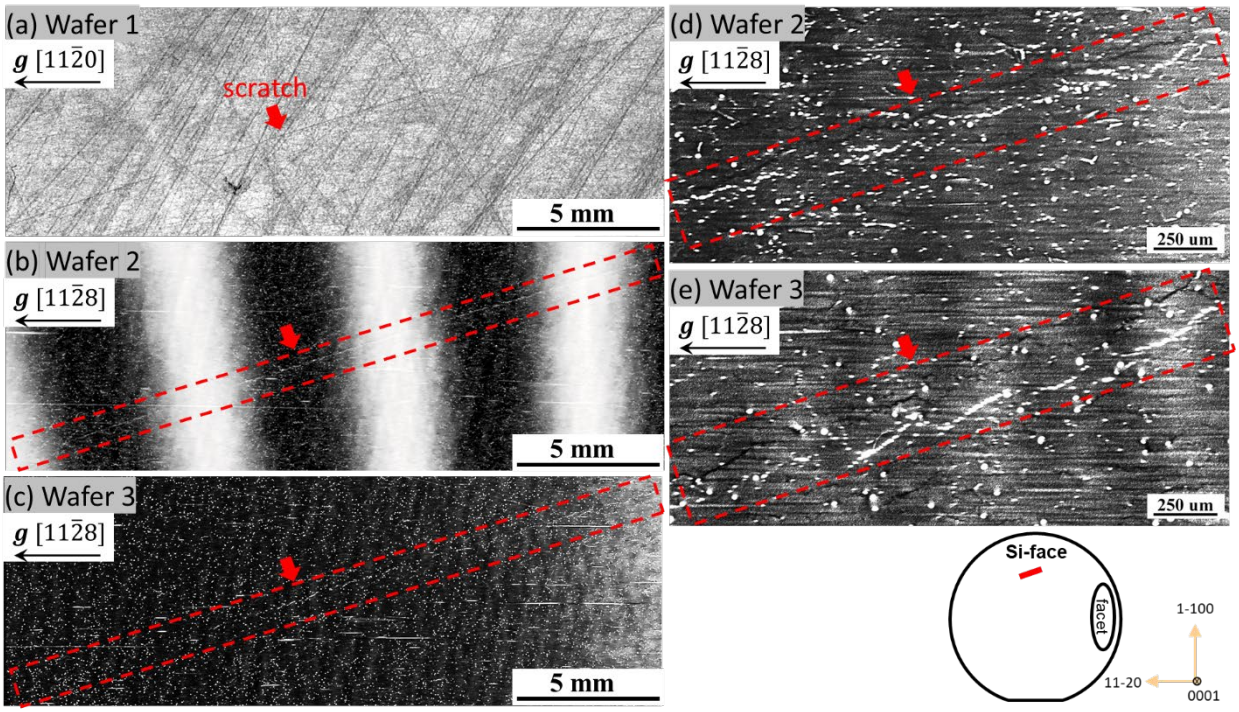

Fig. 7. Synchrotron X-ray topographic observation of a scratch on Wafer 1 (a); and the correlated TED array on Wafer 2 (b, d); and TED LAGB on Wafer 3 (c, e). The location of this feature is at the upper inner region of the wafer indicated by the red line shown on the inset schematic diagram. The dislocation density of this TED array/LAGB decreased from 32223 cm^{-2} in Wafer 2 to 20165 cm^{-2} in Wafer 3.

While most of the scratch induced TED arrays at the inner region are found transformed into TED LAGB at later grown crystal, a TED array found on the lower right edge of Wafer 2 generated from seed scratch is observed to be converted into BPD LAGB in Wafer 3 (Fig. 8). These higher density of BPDs could propagate into epitaxial layers and cause device degradation.

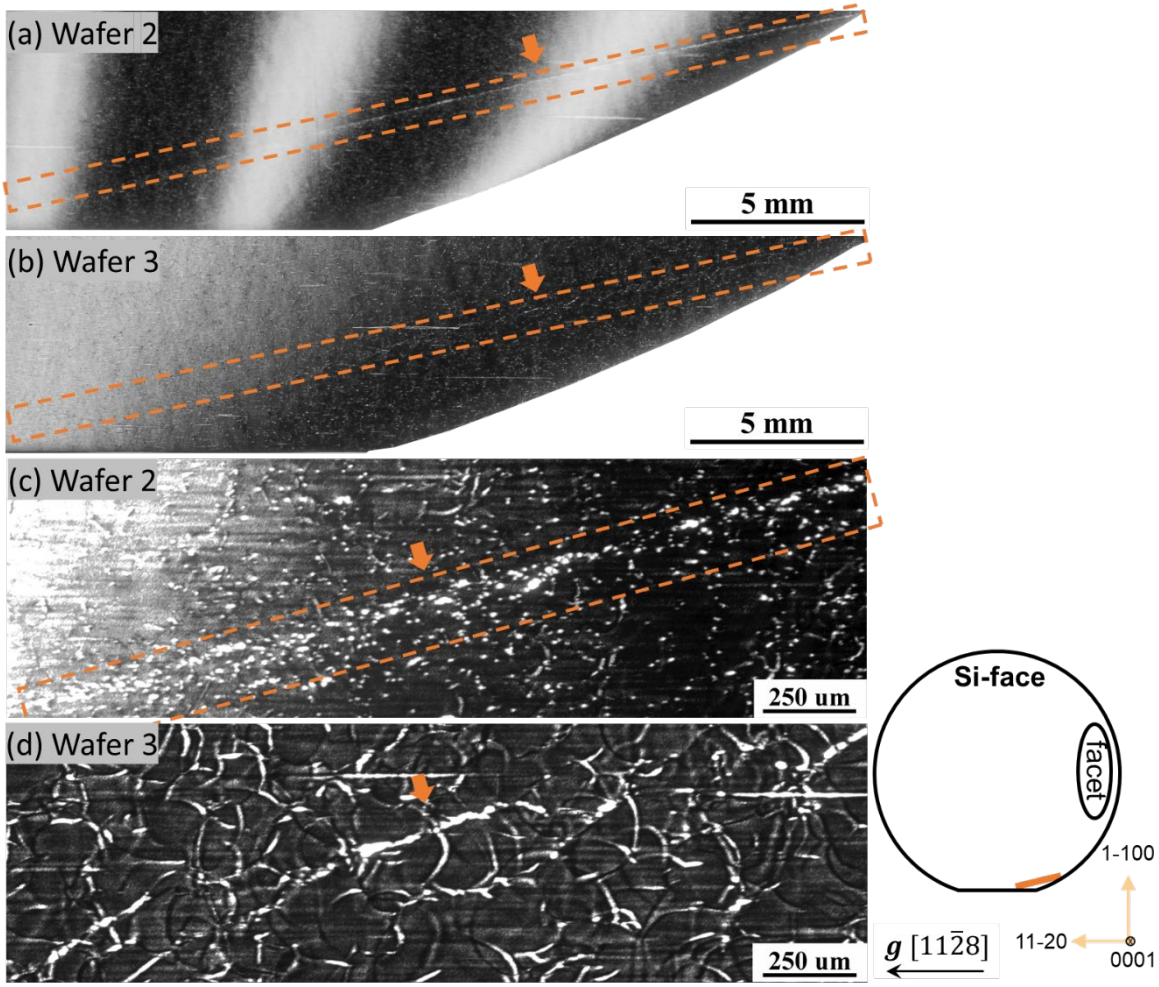

Fig. 8. Synchrotron X-ray topographic observation of a scratch induced TED array on Wafer 2 (a, c); and the correlated BPD LAGB it evolved into on Wafer 3 (b, d). The location of this feature is at the lower right edge of the wafer indicated by the orange line shown on the inset schematic diagram.

Dislocation Nucleation and Evolution Mechanism. Surface damage such as scratches on the seed crystal cause discontinuity on the crystal surface that is accommodated by generating dislocation loops [20, 21]. Depending on the variation of the magnitude and direction of the applied force creating the scratch, dislocation loops generated can be either Frank dislocation half loops or BPD-half loops (Fig. 9a) that subsequently leads to the nucleation of TSDs/TMDs or TEDs connected by those dislocation loops. Since the net Burgers vector must be zero to satisfy the Burgers vector conservation law, dislocations are nucleated as opposite-signed pairs. For Frank dislocation half loops, the two intersecting points with the crystal surface will generate TSDs/TMDs during growth process. For BPD-half loops, the intersecting points may have either edge or screw orientation. Those can lead to the nucleation of TEDs or screw-type BPDs on the newly grown crystal (Fig. 9b). Such dislocation nucleation mechanism will result in the formation of TSD/TMD arrays or TED arrays in the newly grown crystal along the scratch orientation. During PVT growth of the boule, those opposite-signed dislocation pairs of the TSD/TMD or TED array can be annihilated [22] or get deflected onto the basal plane as Frank-type dislocations or BPDs by macro-steps [23] (Fig. 10). This explains the more separated distribution of individual dislocations and decreased dislocation density of TSD/TMD or TED arrays in Wafer 3.

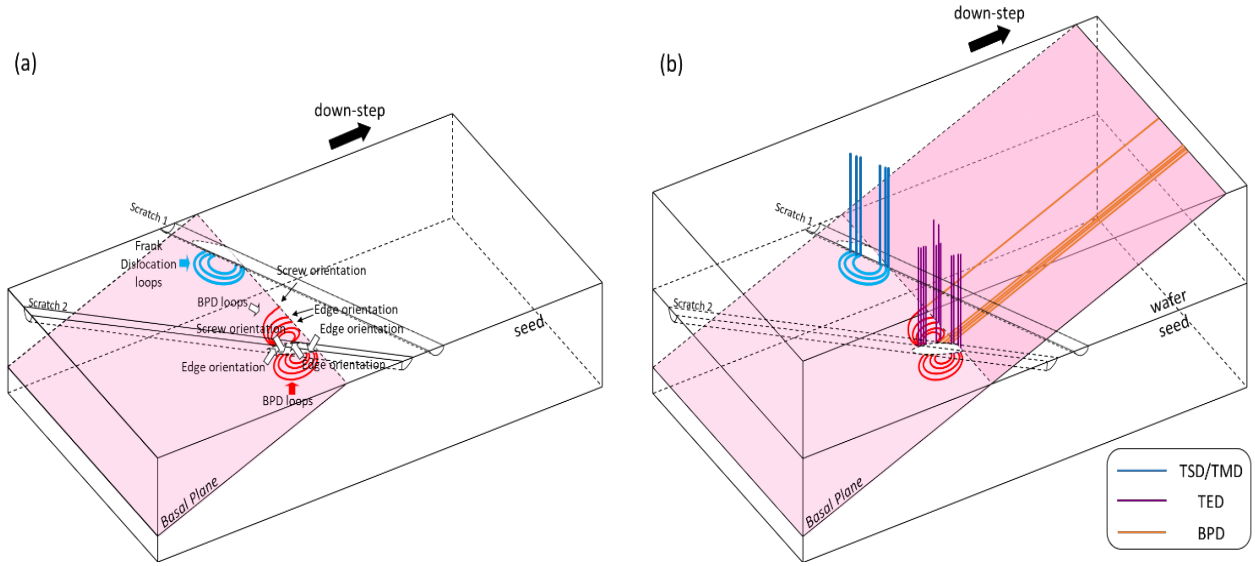

Fig. 9. Schematic diagram showing (a) the generation of dislocation loops due to the seed surface scratch, and (b) the nucleation and propagation of dislocations from the seed crystal into the newly grown wafer.

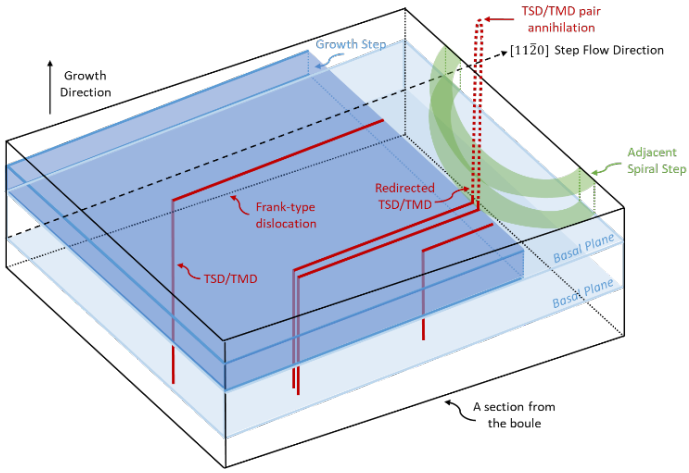

Fig. 10. Schematic diagram showing TSDs/TMDs being deflected onto the basal plane by macro-growth step, they can be redirected back to the threading direction as they encounter an adjacent step from the opposite step flow direction. Threading dislocations with opposite-signed Burgers vectors can be annihilated at a later growth process.

For TED arrays located near wafer periphery, the overgrowth of macro-steps dominates, resulting in deflections of the original threading orientated dislocations on to the basal plane. The resultant BPDs undergo glide and climb to form BPD LAGB through polygonization [24]. As for TED arrays located in the inner regions of the wafer, the effect of macro-step is less significant, which enables the TEDs to propagate into the newly grown crystal while maintaining their threading configuration. Those TEDs can glide during the growth process and tend to align in the energetically favorable direction $< 1\bar{1}00 >$ for tilt boundary formation. Besides, a TED array can also act as a barrier that leads to the accumulation of local BPDs, which further results in the formation of a BPD LAGB. This is observed near the wafer periphery but not the inner region since the BPD density is much higher near the edge compared to inner region of the crystal (approximately 3 to 6 times difference for these three wafers), which makes this barrier effect less significant and no BPD LAGB formation due to TED arrays in the inner region.

Summary

This study investigated the crystal defect nucleation caused by damage from surface scratches not completely removed during polishing on seed crystal and the dislocation propagation and conversion mechanisms during later growth stages. Analysis of the synchrotron white and monochromatic beam X-ray topographs reveals the generation of dislocation arrays composed of TSD/TMD or TED pairs

associated with the scratches in the newly grown wafer adjacent to the seed. All dislocations induced by scratches are initially closely spaced and can be observed as distinct linear features positioned at the exact location of the original seed scratch. Due to the overgrowth of macro-steps as well as the annihilation of opposite-signed pairs during the growth process, TSD/TMD arrays are dispersed wider and less dense in the later grown wafer and TED arrays in the inner region are transform into TED LAGBs with lowered dislocation densities. Near the edge of the wafer, a TED array is converted into a BPD LAGB due to the combined effect of macro-step overgrowth and higher BPD densities in the outer region of the crystal.

Acknowledgement

Work supported by and samples provided by SK siltron css. Research used resources of the Advanced Photon Source (Beamline 1-BM), a U.S. DOE Office of Science User Facility operated for the DOE Office of Science by Argonne National Laboratory under Contract No. DE-AC02-06CH11357. The Joint Photon Sciences Institute at SBU provided partial support for travel and subsistence at the Advanced Photon Source.

References

[1] C. Codreanu et al, Mater Sci Semicond Process 3, 137-142 (2000).

[2] P. G.Neudeck et al, Solid-State Electronics 42(12), 2157-2164 (1998).

[3] P. Bergmanet al, Mater. Sci. Forum 353-356, 299-302 (2001).

[4] A. K. Agarwal et al, IEEE Electron Device Lett. 28, 587-589 (2007).

[5] J. W. Sun et al, Journal of Applied Physics 111(11), 113527 (2012).

[6] R. Singh and M. Pecht, IEEE Industrial Electronics Magazine, 2, 19-31, (2008).

[7] Lely, A.J., Darstellung von Einkristallen von Siliziumcarbid und Beherrschung von Art und Menge der eingebauten Verunreinigungen. Ber. Dtsch. Keram. Ges. 32: 229-231(1955).

[8] D. R. Hamilton, The Growth of Silicon Carbide by Sublimation, in Silicon Carbide, in A High Temperature Semiconductor, J.R. Connor and J. Smilestens, Editors, Oxford: Pergamon. 45-51 (1960).

[9] V. P. Novikov and V.I. Ionov, Production of Monocrystals of Alpha Silicon Carbide. Growth Crystal 6, 9-21 (1968).

[10] Y. M. Tairov and V.F. Tsvetkov, Journal of Crystal Growth 43(2), 209-212 (1978).

[11] X.R. Huang et al, J. Appl. Cryst. 32, 516-524 (1999).

[12] M. Dudley et al, J. Phys. D: Appl. Phys. 32, A139-A144 (1999).

[13] T. Zhou et al, MRS Online Proc. Libr. 1494, 121-126 (1999).

[14] T. Zhou et al, Journal of Elec Materi 43, 838-842 (2014).

[15] Q. Cheng et al, J. Electron. Mater. 50, 4104-4117 (2021).

[16] B. Raghothamachar et al, J. Cryst. Growth 544, 125709 (2020).

[17] H. Peng et al, J. Appl. Cryst. 55, 544-550 (2022).

[18] Q. Cheng et al, Defect and Diffusion Forum 426, 57-64 (2023).

[19] Q. Cheng et al, Materials Science in Semiconductor Processing 174, 108207 (2024).

[20] M. R. Surowiec and B. K. Tanner, Philos. mag., A 55:6, 791-805 (1987).

[21] H. Wang, Studies of Growth Mechanism and Defect Origins in 4H-Silicon Carbide Substrates and Homoepitaxial Layers. 2014. Stony Brook University, PhD dissertation.

[22] K. Kamei et al, Mater. Sci. Forum, 717-720, 45-48 (2012).

[23] T. Ailihumaer et al, J. Electron. Mater., 50, 3258-3265 (2021).

[24] Y Chen et al, Mater. Sci. Forum 556-557, 231-234 (2007).